A multiphase model for concrete: numerical solutions and applications

BERNHARD A. SCHREFLER, FRANCESCO PESAVENTO
Department of Structural and Transportation Engineering
University of Padova
Via F. Marzolo 35131, Padova
ITALY
bas@dic.unipd.it, pesa@dic.unipd.it, http://www.dic.unipd.it

DARIUSZ GAWIN
Department of Building Physics and Building Materials
Technical University of Lodz
Al. Politechniki 6, 93-590 Lodz
POLAND
gawindar@p.lodz.pl http://kfb-lx.p.lodz.pl/darekg_pl.html

Abstract: - A mathematical and numerical model to predict the non-linear behaviour of concrete as multiphase porous material is proposed. The model can be usefully applied to several practical cases: evaluation of concrete performance in the high temperature range, e.g. during fire, to early stages of maturing of massive concrete structures, to shotcrete in tunnelling, and to durability. All the important phase changes of water and chemical reactions, i.e. adsorption-desorption, condensation-evaporation, and hydration-dehydration, as well as the related heat and mass sources or sinks are considered. Changes of the material properties caused by temperature and pressure changes, concrete damage or carbonation, fresh concrete hardening, as well as coupling between thermal, hygral and mechanical phenomena are taken into account. This model further allows to incorporate sorption hysteresis. Some relevant applications of the model will be shown in this work.

Key-Words: Concrete, High Temperature, Damage, Creep, Hydration, Shrinkage, Effective Stress.

1 Introduction

In several situations it is necessary to model concrete as a multiphase material, i.e. a material made up of a solid phase and pores which are filled with water (capillary and physically adsorbed), vapour and dry air. Typical cases deal with concrete performance in the high temperature range, e.g. during fire, with early stages of maturing of massive concrete structures with shotcrete in tunnelling, and with durability.

We present here a general model for chemo-hygro-thermo-mechanical analysis of concrete applicable to the above situations using a mechanistic approach.

Such a kind of approach leads to governing equations that are usually more complicated formally, but their coefficients have clear physical meaning and often are related to classical material parameters, like for example porosity, intrinsic permeability, diffusivity of vapour in air, etc. When some relations between structure parameters and transport properties are found (e.g. effect of water degree of saturation on relative permeability for water flow), usually they are valid for a class of similar materials, e.g. cellular concrete, ceramic materials, etc. Often models of this group are obtained from microscopic balance equations written for particular constituents of the medium, which are then averaged in space, e.g. by means of Volume Averaging Technique, mixture theory or homogenisation theory. Mass and energy fluxes are usually expressed by means of gradients of thermodynamic potentials causing them, e.g. temperature, capillary pressure, water vapour concentration etc. Phase changes and the related mass- and energy sources (sinks) are usually taken into account. Moreover, some additional couplings, e.g. effect of material damaging on intrinsic permeability or capillary and vapour pressures (moisture content) on skeleton stresses, can be considered.

In this paper the model mentioned above is applied to the case of concrete at early ages and beyond and to the case of concrete structures under fire.

2 Physical and mathematical model

Moist concrete is modelled as a multi-phase material, which is assumed to be in thermo-dynamic equilibrium state locally. The voids of the skeleton are filled partly with liquid water and partly with a gas phase. The liquid phase consists of bound water, which is present in the whole range of moisture content, and capillary water, which appears when

water content exceeds the upper limit of the hygroscopic region, S_{ssp}. The gas phase is a mixture of dry air and water vapour, and is assumed to be an ideal gas. The chosen primary variables of the model are: gas pressure p^g, capillary pressure $p^c = p^g - p^w$ (p^w denotes water pressure), temperature T, displacement vector of the solid matrix $\mathbf{u}$, and finally carbon dioxide concentration ρ_d if carbonation process is considered, while the internal variables are: degree of cement hydration Γ_{hydr}, when hydration or dehydration phenomena are analysed, degree of carbonation Γ_{carb}, when carbonation is taken into account and mechanical damage d and thermo-chemical damage V when damaging-deterioration processes are considered. Hence, the general mathematical model of chemo-hygro-thermo-mechanical processes consists of four or five balance equations, depending on the problem analysed. They are completed by an appropriate set of constitutive and state equations, and some thermodynamic relationships. Considering that in this work we do not take into account the case of concrete subjected to carbonation phenomenon (durability mechanics) and that in the case of concrete structures exposed to high temperatures in the range below 600-700°C we can neglect the term related to decarbonation process, the final form of the set of governing equations is:

- Mass balance equation of the dry air

$$-n\frac{D^s S_w}{Dt}-\beta_s(1-n)S_g\frac{D^s T}{Dt}+S_g\,div\,\mathbf{v}^s+\frac{S_g n}{\rho^{ga}}\frac{D^s\rho^{ga}}{Dt}+\frac{1}{\rho^{ga}}div\,\mathbf{J}_g^{ga}+\frac{1}{\rho^{ga}}div\left(n\,S_g\rho^{ga}\mathbf{v}^{gs}\right)+-\frac{(1-n)S_g}{\rho^s}\frac{\partial\rho^s}{\partial\Gamma_{hydr}}\frac{D^s\Gamma_{hydr}}{Dt}=\frac{\dot m_{hydr}}{\rho^s}S_g \quad (1)$$

- Mass balance equation of the water species

$$n\left(\rho^w-\rho^{gw}\right)\frac{D^s S_w}{Dt}+\left(\rho^w S_w+\rho^{gw}S_g\right)\alpha\,div\,\mathbf{v}^s+ +div\,\mathbf{J}_g^{gw}+div\left(n\,S_w\rho^w\mathbf{v}^{ws}\right)+div\left(n\,S_g\rho^{gw}\mathbf{v}^{gs}\right)+-\left(\rho^w S_w+\rho^{gw}S_g\right)\frac{(1-n)}{\rho^s}\frac{\partial\rho^s}{\partial\Gamma_{hydr}}\frac{D^s\Gamma_{hydr}}{Dt}+S_g n\frac{D^s\rho^{gw}}{Dt}= =\frac{\dot m_{hydr}}{\rho^s}\left(\rho^w S_w+\rho^{gw}S_g-\rho^s\right) \quad (2)$$

- Enthalpy balance equation of the multi-phase medium

$$\left(\rho C_p\right)_{eff}\frac{\partial T}{\partial t}+\left(\rho_w C_p^w\mathbf{v}^w+\rho_g C_p^g\mathbf{v}^g\right)\cdot grad\,T+ -div\left(\lambda_{eff}\,grad\,T\right)=-\dot m_{vap}\Delta H_{vap}+\dot m_{dehydr}\Delta H_{dehydr} \quad (3)$$

- Linear momentum conservation equation of the multi-phase medium

$$div\left(\boldsymbol{\sigma}_e^s-\alpha p^s\,\mathbf{I}\right)+\rho\mathbf{g}=0 \quad (4)$$

where the effective stresses $\boldsymbol{\sigma}_e^s$ is given by:

$$\boldsymbol{\sigma}_e^s=(1-D)\boldsymbol{\Lambda}_\mathbf{0}:\left(\boldsymbol{\varepsilon}_{tot}-\boldsymbol{\varepsilon}_{th}-\boldsymbol{\varepsilon}_0\right) \quad (5)$$

where the parameter D is the total damage resulting from various material deterioration processes of different nature: mechanical, thermo-chemical, purely chemical.

The term $\boldsymbol{\varepsilon}_0$ in eq. (5) is formed by two different contributions: chemical strains accounting for thermo-chemical deterioration process in case of elevated temperatures or chemical reactions in all the other cases, and creep strains accounting for mid-long term creep in durability problems and thermal creep in high temperature ranges:

$$\boldsymbol{\varepsilon}_0=\boldsymbol{\varepsilon}_{chem}+\boldsymbol{\varepsilon}_{creep} \quad (6)$$

The mass balance equation of carbon dioxide has to be added to the previous ones if carbonation phenomenon is analysed. Furthermore, three (or more) evolution equations, corresponding to the internal variables related to the evolution processes included in the model, can be added to the above described governing equations:

- Hydration/Dehydration process evolution law

When dehydration process is considered (temperature higher than 105°C), taking into account its irreversibility, one may assume that the degree of dehydration depends on the maximum value of temperature reached during heating:

$$\Gamma_{dehydr}(t)=\Gamma_{dehydr}\left(T_{max}(t)\right) \quad (7)$$

while, when hydration process is analyzed (below 105°C) the hydration degree is defined in the following way:

$$\Gamma_{hydr}=\frac{\chi}{\chi_\infty}=\frac{m_{hydr}}{m_{hydr\infty}} \quad (8)$$

where m_{hydr} means mass of hydrated water (chemically combined), χ is the hydration extent and χ_∞, $m_{hydr\infty}$ are the final values of hydration extent and mass of hydrated water, respectively.

- Thermo-chemical damage evolution equation (high temperature)

The parameter V takes into account both effects of concrete dehydration (chemical component) and material cracking (mechanical component) on material degradation and the Young's modulus decrease with increasing temperature. It is obtained from the experimental results, and is a function of the maximum temperature reached during heating because of the irreversible character of the material structural changes:

$$V(t) = V\left(T_{max}(t)\right) \tag{9}$$

- Mechanical damage evolution equation

The mechanical damage parameter d is expressed in terms of the equivalent strain, $\tilde{\varepsilon}$, and it is given by equations of the classical non-local, isotropic damage theory,

$$d(t) = d\left(\tilde{\varepsilon}(t)\right) \tag{10}$$

Similarly to what has been stated for governing equations, if carbonation process is taken into account in the modelling of concrete behaviour, it is necessary to define the corresponding evolution equation. For a full description of the model and its mathematical formulation, see [1]-[5].

3 Numerical solution

The governing equations of the model (1)-(5) are discretised in space by means of the finite element method, [1,6]. The unknown variables are expressed in terms of their nodal values as,

$$\begin{aligned} p^g(t) &\cong \mathbf{N}_p\,\overline{\mathbf{p}}^g(t), \qquad p^c(t) \cong \mathbf{N}_p\,\overline{\mathbf{p}}^c(t), \\ T(t) &\cong \mathbf{N}_t\,\overline{\mathbf{T}}(t), \qquad \mathbf{u}(t) \cong \mathbf{N}_u\,\overline{\mathbf{u}}(t). \end{aligned} \tag{11}$$

The variational or weak form of the model equations, was obtained in [1,5] by means of Galerkin's method (weighted residuals), and can be written in the following concise discretised matrix form,

$$\mathbf{C}_{ij}(\mathbf{x})\frac{\partial \mathbf{x}}{\partial t} + \mathbf{K}_{ij}(\mathbf{x})\,\mathbf{x} = \mathbf{f}_i(\mathbf{x}), \qquad \text{with} \tag{12}$$

$$\mathbf{f}_i = \begin{Bmatrix} \mathbf{f}_g \\ \mathbf{f}_c \\ \mathbf{f}_t \\ \mathbf{f}_u \end{Bmatrix}, \mathbf{K}_{ij} = \begin{bmatrix} \mathbf{K}_{gg} & \mathbf{K}_{gc} & \mathbf{K}_{gt} & \mathbf{0} \\ \mathbf{K}_{cg} & \mathbf{K}_{cc} & \mathbf{K}_{ct} & \mathbf{0} \\ \mathbf{K}_{tg} & \mathbf{K}_{tc} & \mathbf{K}_{tt} & \mathbf{0} \\ \mathbf{K}_{ug} & \mathbf{K}_{uc} & \mathbf{K}_{ut} & \mathbf{K}_{uu} \end{bmatrix},$$
$$\mathbf{C}_{ij} = \begin{bmatrix} \mathbf{C}_{gg} & \mathbf{C}_{gc} & \mathbf{C}_{gt} & \mathbf{C}_{gu} \\ \mathbf{0} & \mathbf{C}_{cc} & \mathbf{C}_{ct} & \mathbf{C}_{cu} \\ \mathbf{0} & \mathbf{C}_{tc} & \mathbf{C}_{tt} & \mathbf{C}_{tu} \\ \mathbf{0} & \mathbf{0} & \mathbf{0} & \mathbf{0} \end{bmatrix}, \tag{13}$$

where the vectors $\mathbf{x}^T = \left\{\overline{\mathbf{p}}^g, \overline{\mathbf{p}}^c, \overline{\mathbf{T}}, \overline{\mathbf{u}}\right\}$ and $\mathbf{f}_i(\mathbf{x})$ and the non-linear matrices $\mathbf{C}_{ij}(\mathbf{x})$, $\mathbf{K}_{ij}(\mathbf{x})$ are defined in detail in [1-5]. The time discretization is accomplished through a fully implicit finite difference scheme (backward Euler),

$$\Psi^i\left(\mathbf{x}_{n+1}\right) = \mathbf{0},$$

$$\Psi^i\left(\mathbf{x}_{n+1}\right) = \mathbf{C}_{ij}\left(\mathbf{x}_{n+1}\right)\frac{\mathbf{x}_{n+1} - \mathbf{x}_n}{\Delta t} + \tag{14}$$
$$+\mathbf{K}_{ij}\left(\mathbf{x}_{n+1}\right)\mathbf{x}_{n+1} - \mathbf{f}_i\left(\mathbf{x}_{n+1}\right)$$

where superscript i (i= g,c,t,u) denotes the state variable, n is the time step number and Δt the time step length.

The non-linear equation set (14) is linearised and solved by means of a monolithic Newton-Raphson type iterative procedure [1-6]:

$$\Psi^i\left(\mathbf{x}_{n+1}^k\right) = -\left.\frac{\partial \Psi^i}{\partial \mathbf{x}}\right|_{\mathbf{x}_{n+1}^k} \Delta\mathbf{x}_{n+1}^k, \quad \mathbf{x}_{n+1}^{k+1} = \mathbf{x}_{n+1}^k + \Delta\mathbf{x}_{n+1}^k, \tag{15}$$

where k is the iteration index and $\dfrac{\partial \Psi^i}{\partial \mathbf{x}}$ is Jacobian matrix.

4 Application of the model to concrete at early ages

From the macroscopic point of view, hydration of cement is a complex interactive system of competing chemical reactions of various kinetics and amplitudes. They are associated with complex physical and chemical phenomena at the micro-level of material structure, see e.g. [7,8], resulting in considerable changes of macroscopic concrete properties. Kinetics of cement hydration (hydration rate) cannot be described properly in terms of equivalent age nor maturity of concrete, if the effect of the reaction rate on temperature (and/or relative humidity) depends upon the hydration degree [7], or chemical affinity of the reaction is affected by temperature variations (and/or relative humidity) [9]. Hence, another thermodynamically based approach has been used instead, similarly as proposed by Ulm and Coussy [10,11], see [4,5]. In this approach the hydration extent χ is the advancement of the hydration reaction and its rate is related to the affinity of the chemical reaction through an Arrhenius-type relationship, as usual for thermally activated chemical reactions, [4,5]:

$$\frac{d\chi}{dt} = \tilde{A}_\chi(\chi)\exp\left(-\frac{E_a}{RT}\right) \tag{16}$$

where $\tilde{A}_\chi(\chi)$ is normalized affinity (it accounts both for chemical non-equilibrium and for the nonlinear diffusion process), E_a – hydration activation energy, and R – universal gas constant. Equation (16) can be rewritten in terms of hydration degree, defined as in eq. (8), and relative humidity by means of a function $\beta_\varphi(\varphi)$, (φ is the relative humidity), [4,5]:

$$\frac{d\Gamma_{hydr}}{dt} = \tilde{A}_\Gamma\left(\Gamma_{hydr}\right)\beta_\varphi(\varphi)\exp\left(-\frac{E_a}{RT}\right) \tag{17}$$

An analytical formula for the description of the normalized affinity of the following form,

$$\tilde{A}_\Gamma\left(\Gamma_{hydr}\right) = A_1\left(\frac{A_2}{\kappa_\infty} + \kappa_\infty\Gamma_{hydr}\right)\left(1-\Gamma_{hydr}\right)\exp\left(-\overline{\eta}\,\Gamma_{hydr}\right) \tag{18}$$

was proposed by Cervera et al. [12] and is used in our model, [4,5]. The coefficients A_1, A_2 and $\overline{\eta}$ can

be obtained from the temperature evolution during adiabatic tests. As far as creep is concerned, fresh concrete is modelled as a visco-elastic material by use of the rate (incremental) formulation of solidification theory [13,14]. In this theory concrete maturing is attributed to a growth of the volume fraction of load-bearing hydrated cement, which itself is considered as a non-aging visco-elastic material. Usually, the creep on these non-aging constituents is described by a Kelvin chain with a finite number N of Kelvin units. In this case the spectrum is discrete and its identification from test data is an ill-posed problem. To overcome this problem a continuous retardation spectrum has been introduced into the model. This means that a continuous Kelvin chain model with infinitely many Kelvin units and retardation times spaced infinitely closely, has been used [4,5,14].

It is important to underline that we model hygro-mechanical interactions (i.e. capillary shrinkage phenomenon) using effective stresses defined as, [4,5]:

$$\boldsymbol{\sigma}_e^s = \boldsymbol{\sigma} + \alpha p^s \mathbf{I}, \tag{19}$$

where α is the Biot's constant and p^s is the solid pressure:

$$p^s = \chi_s^{ws}\left(p^w + s^{ws} J_{ws}^s\right) + \left(1-\chi_s^{ws}\right)\left(p^g + s^{gs} J_{gs}^s\right) \tag{20}$$

where χ_s^{ws} is the fraction of skeleton area in contact with water, J_{ws}^s, J_{gs}^s the average curvatures of the solid-water and solid-gas phase interfaces, respectively, obtained by integrating the point curvature over the interface within the macro scale volume, and s^{ws}, s^{gs} are interfacial tension like terms. Solid pressure accounts for the pressure exerted by pore fluids on solid skeleton. This component of the stress tensor causes an additional deformation of the skeleton (shrinkage strains), hence one can expect that it will contribute to creep strains, as well [4,5]. Indeed, some experimental studies of autogenous deformations of concrete at early ages, e.g. [15], suggest that a part of the material strains in such a situation (i.e. without any external load) can be explained only by creep deformations due to capillary forces.

4.1 Numerical simulation of self-desiccation process

The numerical example deals with self-heating and self-desiccation phenomena in sealed, cylindrical concrete samples made of ordinary and HPC concretes (60 cm long and with diameter of 4 cm), placed in adiabatic conditions. These specimens have been used for testing of autogenous relative humidity change and autogenous deformation, during first 30 days of concrete maturing. The simulation results are compared with available experimental data concerning temperature changes during cement hydration.

The deformation is usually measured in a middle part of a sample, which is unaffected by edge effects, hence the element performance is modeled as a 1-D axisymmetric problem. The mesh with 26 (26x1) eight-node serendipity finite elements of variable sizes (decreasing towards to the surface and to the axis) was used for space discretisation of the sample. Simulations were performed for two types of concrete: OC tested by Bentz et al. [16] and HPC tested by Laplante [17], which were also used by Cervera et al. [12] for validation of their thermo-chemo-mechanical model of concrete at early ages. The composition of these two types of concrete were similar to those used by Baroghel-Bouny et al. [18] during their measurements of hygral properties, i.e. sorption isotherms, intrinsic and relative permeability, thus we assumed these data in our simulations, [4]. Main material properties (for dry concrete after 28-days of maturation) used in our calculations are summarized in Table 1. The heat and mass sources related to concrete maturing are expressed as a function of the hydration rate by means of relation (17), where normalized affinity was described by (18) with the parameters determined in [12,19], see Table 1. Initially, the cylinder has a temperature T_0 =293.15 K and relative humidity φ_0=99.9% for OC, while φ_0=99.0% for HPC. It is assumed that the hydration process started about 2-3 hours before, hence the sample had already a certain shape rigidity and initial hydration degree was equal to 0.1. The external surfaces of the sample are sealed and adiabatic. Results of our simulations concerning the changes of temperature, relative humidity and degree of hydration during initial stages of concrete maturing are shown in Figures 1 and 2 for OC and HPC. In HP concrete we observe considerably lower values of relative humidity at initial stages of maturing, that shows for HPC concrete an influence of relative humidity on the hydration process and the related autogenous changes of temperature and moisture content (i.e. self-heating and self-desiccation phenomena) are of importance. The temperature histories for the analyzed types of concrete are compared to the experimental results from literature [16,17], showing their good agreement. The temperatures obtained from simulations for HPC for time $t > 12h$ are visibly higher than the experimental ones, what is caused by not perfectly adiabatic conditions during the test, as mentioned in [19].

Table 1. Characteristic properties of different types of concrete (in dry state, after 28 days of maturing) used in numerical simulations.

Parameter	Symbol	Unit	OC	HPC
Water/cement ratio	w/c	[-]	0.45	0.35
Aggregate/cem. ratio	c/a	[-]	4.0	4.55
Silica fume/cem. ratio	s/a	[-]	0.00	0.09
Porosity	n	[%]	12.2	8.2
Intrinsic permeability	k	[m^2]	$3 \cdot 10^{-18}$	$1 \cdot 10^{-18}$
Activation energy	E_a/R	[K]	5000	4000
Param. A_1 in eq. (13)	A_1	[1/s]	$7.78 \cdot 10^{4}$	$1.11 \cdot 10^{3}$
Param. A_2 in eq. (13)	A_2	[-]	$0.5 \cdot 10^{-5}$	$1 \cdot 10^{-4}$
Param. κ_∞ in eq. (13)	κ_∞	[-]	0.72	0.58
Param. $\overline{\eta}$ in eq. (13)	$\overline{\eta}$	[-]	5.3	6.0 (4.7)
Thermal conductivity	λ_{eff}	[W/mK]	1.5	1.78
Young's modulus	E	[GPa]	24.11	39.61
Compressive strength	f_c	[MPa]	26	70

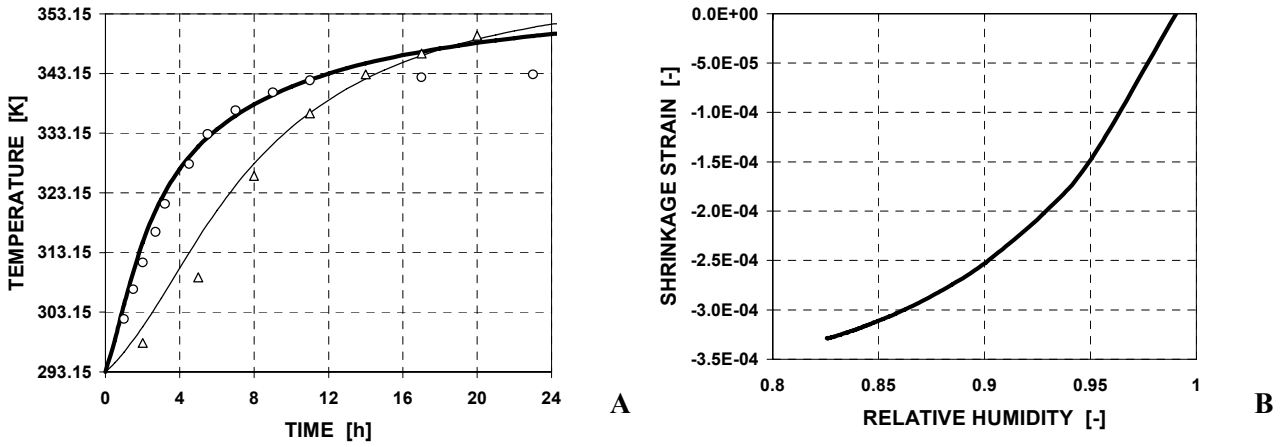

Fig. 1: Thin line: Ordinary concrete; solid line: High Performance Concrete: A) Temperature history in the specimen (and comparison with experimental results), B) Shrinkage strains versus Relative Humidity in HPC sample.

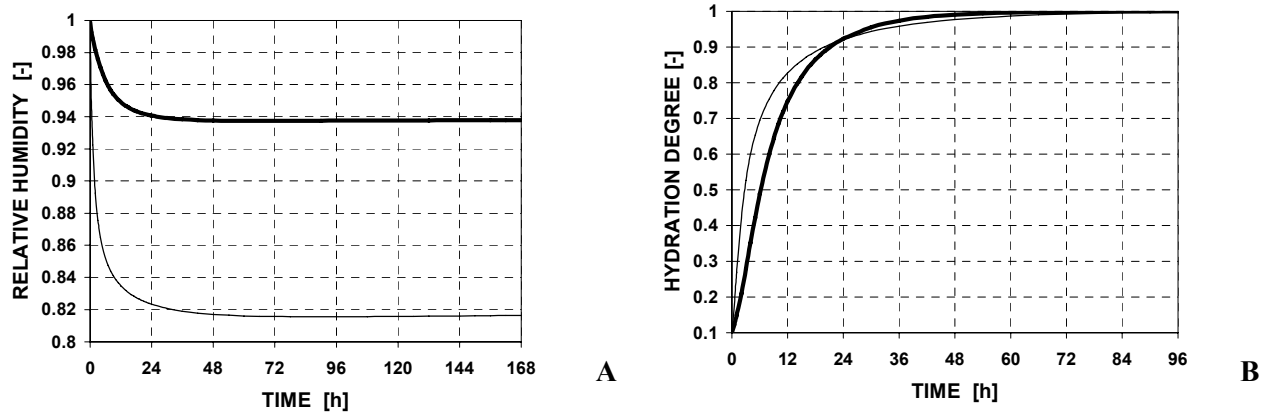

Fig. 2: Thin line: Ordinary concrete; solid line: High Performance Concrete: A) Relative Humidity history, B) Hydration degree history

5 Application of the model to concrete structures in high temperature environments

The model has been applied to the analysis of behaviour of concrete structures under severe temperatures and pressures.

In these conditions concrete structures experience spalling phenomenon, which results in rapid loss of the surface layers of the concrete at temperature exceeding about 200-300°C. As a result, the core concrete is exposed to these temperatures, thereby increasing the rate of heat transmission to the core part of the element and in particular to the reinforcement, what may pose a risk for the integrity of concrete structure.

It is commonly believed that the main reasons of the thermal spalling are: build-up of high pore pressure close to the heated concrete surface as a result of rapid evaporation of moisture, and the release of the stored energy due to the thermal stresses resulting from high values of restrained strains caused by temperature gradients. Nevertheless, relative importance of the two factors is not established yet and still needs further studies, both experimental and theoretical.

The results of the research performed up to now show, that the fire performance of concrete structures is influenced by several factors, like initial moisture content of the concrete, the rate of temperature increase (fire intensity), porosity (density) and permeability of the concrete, its compressive strength, type of aggregate, dimensions and shape of a structure, its lateral reinforcement and loading conditions. The HSC structures are particularly affected by this phenomenon. In fact, HSC provides better structural performance, especially in terms of strength and durability, compared to traditional, normal-strength concrete (NSC).

However, many studies, showed that the fire performance of HSC differs from that of NSC which exhibits rather good behaviour in these conditions.

An unloaded sample of plain concrete or cement stone, exposed for the first time to heating, exhibits considerable changes of its chemical composition, inner structure of porosity and changes of sample dimensions (irreversible in part). The concrete strains during first heating, called load-free thermal strains (LFTS), [20], are usually treated as superposition of thermal and shrinkage components, and often are considered as almost inseparable. LFTS are decomposed in three main contributions, [21]:

- *Thermal dilatation strains,*

$$d\boldsymbol{\varepsilon}_{th} = \beta_s(T)\, dT \tag{21}$$

- *Capillary shrinkage strains,*

$$d\boldsymbol{\varepsilon}_{sh} = \frac{\alpha}{K_T}\left(dx_s^{ws} p^c + x_s^{ws} dp^c\right)\mathbf{I} \tag{22}$$

where K_T is the bulk modulus of the porous medium,

- *Thermo-chemical strains*

$$d\boldsymbol{\varepsilon}_{tchem} = \beta_{tchem}(V)\, dV \tag{23}$$

where $\beta_{tchem}(V) = \dfrac{\partial \boldsymbol{\varepsilon}_{tchem}(V)}{\partial V}$ is obtained from experimental tests (V is the thermo-chemical damage parameter).

As far as the first contribution is concerned, the strains are treated in a manner usual in thermo-mechanics, but considering the thermal expansion coefficient β_s as a function of temperature.

Shrinkage strains are modelled by means of the effective stress principle in the form derived in [1-5], eq. (19), which for materials with very small pores and well developed internal pore surface, where water is also present as a thin film (like for example in concrete), presents a coefficient x_s^{ws} instead of the classical saturation S.

In this way, the (capillary) shrinkage represents a load for the skeleton of the material and the related strains are not computed directly in the strain decomposition as it is usual in the classical phenomenological approaches. This coefficient is a function of saturation S and takes into account the disjoining pressure which is important in the range of saturation in which only a thin film of water is adsorbed to the wall of the pores. This treatment of the shrinkage strains is more consistent from thermodynamic point of view.

In heated concrete, above the temperature of about 105°C, the thermal decomposition of the cement matrix takes place, and at higher temperatures also that of aggregate (depending on its type and composition). This is a consequence of several complicated, endothermic chemical reactions, called concrete dehydration. As their result a considerable shrinkage of cement matrix (called chemical shrinkage) and usually expansion of aggregate are observed. Due to these contradictory behaviour of the material components, cracks of various dimensions are developing when temperature increases, causing an additional change of concrete strains (usually expansion). These strains are modelled as function of thermo-chemical damage which takes into account the thermo-chemical deterioration of the material.

Also the so called LITS, [20], has been considered in the computation. During first heating, mechanically loaded concrete exhibits greater strains as compared

to the load-free material at the same temperature. These additional deformations are referred to as load induced thermal strains (LITS), [20,21]. A part of them originates just from the elastic deformation due to mechanical load, and it increases during heating because of thermo-chemical and mechanical degradation of the material strength properties. The time dependent part of the strains during transient thermal processes due to temperature changes, is generally called thermal creep. The formulation employed into the model is due to Thelandersson [22] in its original form, here modified using a coefficient $\overline{\beta}_{tr}(V)$ as a function of thermo-chemical damage V (and not constant) and the effective stresses instead of total stresses, coupling in this way the thermo-chemo-mechanical damage model and capillary shrinkage model with thermal creep model.

$$d\boldsymbol{\varepsilon}_{tr} = \frac{\overline{\beta}_{tr}(V)}{\mathrm{f_c}(T_a)}\mathbf{Q} : \tilde{\boldsymbol{\sigma}}\, dV \tag{24}$$

in eq. (15) $\mathbf{Q}$ is a fourth order tensor, $\tilde{\boldsymbol{\sigma}}$ is the effective (in the sense of damage mechanics) stress tensor and finally f_c is the compressive strength of the material at 20°C.

The model in this form can be successfully applied to several real cases, e.g. the case of fire in tunnels, [23]. For further details see [2-5,24-29].

5.1 Numerical simulation of cylindrical specimen exposed to high temperature

This example deals with a comparison between numerical results, obtained using the model described in the previous sections, and experimental results, obtained from compressive tests carried out in United States in the laboratories of NIST (i.e. National Institute of Standard and Technology) [30-32]. The main goal of this comparison is to show the capability of the code to assess spalling phenomena, in particular occurrence of explosive spalling in concrete structures subjected to elevated temperatures. The specimens were cylinders with diameter of 100 mm and height of 200 mm, have been tested using three test methods, representing the thermo-mechanical loading conditions: stressed test method (specimens were preloaded, with a load equal to 40% of final compressive strength at room temperature, and then heated), unstressed test method (specimens were directly heated until the time of compressive test), residual property test method (the specimens were heated up to the target temperature and kept at this temperature for a certain period; then they were cooled and tested at room temperature, i.e. at residual conditions).

Five target temperatures: 100°C, 200°C, 300°C, 450°C and 600°C were reached during the tests by means of furnace heating rate of 5°C/min, in steady state conditions. In this case "steady state" is defined as the temperature state when the temperature at the centre of the specimen is within 10°C of the pre-selected target temperature T and the difference between the surface and centre temperatures of the concrete specimen is less than 10°C. For further details concerning mix compositions and tests procedures (set-up, instrumentation of the specimens, temperature control), see [30-32]. Our attention was focused on specimens made of concrete type 1, herein indicated as MIX1 in unstressed conditions with a target temperature equal to 450°C. In fact, for unstressed tests, explosive spalling occurred in all MIX1 specimens heated to 450°C. Initial and boundary conditions used in numerical simulation are listed in [21]. Fig. 3A shows the temperature differences between the surface and the centre of the specimens measured during the tests and the corresponding numerical results. The accordance between numerical and experimental results is quite good. The first part of heating shows a strange behaviour with temperature difference between core and surface practically zero for more than one hour. Fig. 4B provides information about damaging of the specimen during heating. Specifically, it shows the history of total damage in three different points (on the surface, in the centre and in the middle of the radius). The evolution of creep strain is shown in Fig. 4A for three different points. Fig. 3B shows developments (in three points) of the gas pressure versus temperature compared to the water vapour pressure developments in saturated conditions (red line). The time range between 120 and 150 min seems to be the critical range during which the material achieves a state favourable to spalling occurrence; the specimen experienced explosive spalling right in this range of time. Corresponding to the maximum value of ΔT, a sharp increase of mechanical damage parameter d (with a maximum value equal to 80%) may be observed. Similarly to the increase of mechanical damage, the peak of gas pressure corresponds to the maximum value of temperature differences ΔT. The presented results of numerical simulations, show that both pore pressure and thermally induced strains can be identified as responsible for the spalling occurrence, and that they play a primary or secondary role depending on the particular conditions prevailing. For the analysed HPC concretes, the MIX 1 specimens, having lower value of the w/c ratio, spalled explosively mainly due to the high gas pressure value and relatively high level of thermo-chemical deterioration.

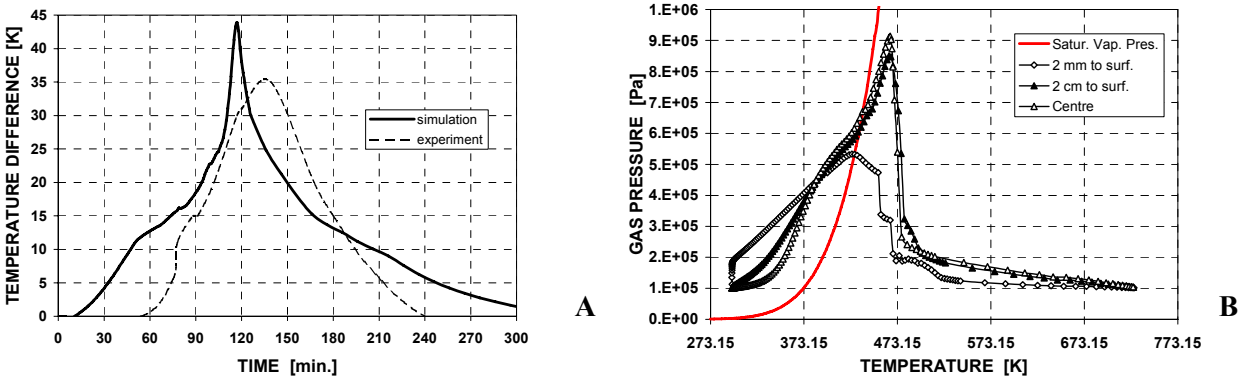

Fig. 3: Cylindrical specimen exposed to high temperature: A) Temperature differences history in the specimen (and comparison with experimental results), B) Gas pressure versus temperature in three different points and saturated vapour pressure (red line).

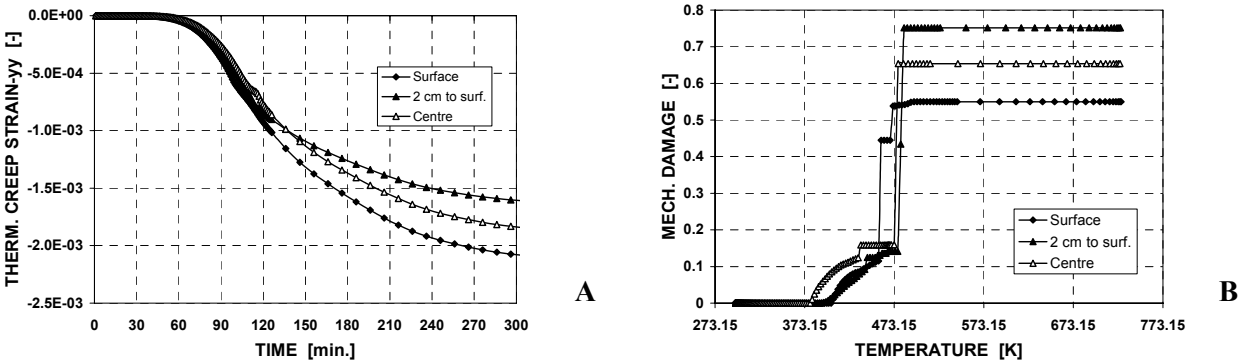

Fig. 4: Cylindrical specimen exposed to high temperature: A) Creep strains history according to eq. (19), B) Mechanical damage versus temperature in three different points.

6 Conclusions

A general model for the non-linear modelling of concrete behaviour has been presented in this work. All relevant mass and heat transport phenomena, chemical reactions, phase changes as well as their mechanical effects are taken into account. The richness of the model allows for its application to several practical cases such as the analysis of hydration and aging processes in massive concrete structures and the analysis of the response of concrete structures exposed to high temperatures.

References:

[1] Lewis R.W., Schrefler B.A., *The Finite Element Method in the Static and Dynamic Deformation and Consolidation of Porous Media*, Wiley & Sons, Chichester, 1998.

[2] Gawin D., Pesavento F., Schrefler B.A., Modelling of hygro-thermal behaviour of concrete at high temperature with thermo-chemical and mechanical material degradation, *Comp. Meth. Appl. Mech. Engrg.*, No 192, 2003, pp. 1731-1771.

[3] Pesavento F., *Non-linear modelling of concrete as multiphase porous material in high temperature conditions*, Ph.D. thesis, University of Padova, Padova, 2000.

[4] D. Gawin, F. Pesavento, B.A. Schrefler, Hygro-thermo-chemo-mechanical modelling of concrete at early ages and beyond. Part I: Hydration and hygro-thermal phenomena, *Int. J. Num. Meth. Engng*, Vol. 67, 2006, pp. 299–331.

[5] D. Gawin, F. Pesavento, B.A. Schrefler, Hygro-thermo-chemo-mechanical modelling of concrete at early ages and beyond. Part II: Shrinkage and creep of concrete, *Int. J. Num. Meth. Engng*, Vol. 67, 2006, pp. 332–363.

[6] Zienkiewicz O.C., Taylor R.L., *The Finite Element Method, vol. 1: The Basis*, Butterworth-Heinemann, Oxford, 2000.

[7] de Schutter G., Taerwe L., General hydration model for Portland cement and blast furnace slag cement, *Cement Concrete Res.*, Vol 25, No 3, 1995, pp. 593-604.

[8] de Schutter G., Influence of hydration reaction on engineering properties of hardening concrete; *Mater. Struct.*, No 35, 2002, pp. 453-461.

[9] Jensen O.M., Hansen P.F., Influence of temperature on autogenous deformation and relative humidity change in hardening cement paste, *Cem. Concr. Res.*, No 29, 1999, pp. 567-575.

[10] Ulm F.-J., Coussy O., Modeling of thermo-chemo-mechanical couplings of concrete at early ages, *J. Eng. Mech.*, ASCE, Vol 121, No 7, 1995, pp. 785-794.

[11] Ulm F.-J., Coussy O., Strength growth as chemo-plastic hardening in early age concrete, *J. Eng. Mech.*, ASCE, Vol 122, No 12, 1996, pp. 1123-1132.

[12] Cervera M., Olivier J., Prato T., A thermo-chemo-mechanical model for concrete. I: Hydration and aging. *ASCE, J. Eng. Mech.*, Vol 125, No 9, 1999, pp. 1018-1027.

[13] Bazant Z.P., Prasannan S., Solidification theory for concrete creep. I: Formulation, II. Verification and application, *J. Engng Mech. ASCE*, Vol 115, 1989, pp. 1691-1725.

[14] Bazant Z.P., Xi Y., Continuous retardation spectrum for solidification theory of concrete creep, *J. Eng. Mech. ASCE*, Vol 121, 1995, pp. 281-288.

[15] Lura P., Jensen O.M., van Breugel K., Autogenous shrinkage in high-performance cement paste: an evaluation of basic mechanisms, *Cem. Concr. Res*. Vol 33, No 2, 2003, pp. 223-232.

[16] Bentz D.P., Waller V., de Larrard F., Prediction of adiabatic temperature rise in conventional and high-performance concretes using a 3-d microstructural model, *Cement Concrete Res*. Vol 28, No 2, 1998, pp. 285-297.

[17] Laplante P., *Mechanical properties of hardening concrete: A comparative analysis of classical and high strength concrete*, (in French), Ph.D. thesis, Ecole Nationale des Pontes et Chaussées, Paris, 1993.

[18] Baroghel-Bouny V., Mainguy M., Lassabatere T., Coussy O., Characterization and identification of equilibrium and transfer moisture properties for ordinary and high-performance cementitious materials, *Cement Concrete Res.*, Vol 29, 1999, pp. 1225-1238.

[19] Cervera M., Olivier J., Prato T., A thermo-chemo-mechanical model for concrete. I: Damage and creep. *ASCE J. Eng. Mech.*, Vol 125, No 9, 1999, pp. 1028-1039.

[20] Khoury G.A., Strain components of nuclear-reactor-type concretes during first heating cycle, *Nuclear Engng and Design*, Vol 156, 1995, pp. 313-321.

[21] Gawin D., Pesavento F., Schrefler B.A., Modelling of deformations of high strength concrete at elevated temperatures, *Materials and Structures/Concrete Science and Engineering*, Vol 37, No 268, 2004 pp. 218-236.

[22] Thelandersson S., Modeling of combined thermal and mechanical action on concrete, *J. Engng Mech, ASCE*, Vol 113, No 6, 1987 pp. 893-906.

[23] Schrefler B.A., Brunello P., Gawin D., Majorana C.E., Pesavento F., Concrete at high temperature with application to tunnel fire, *Comp. Mech.*, Vol 29, 2002, pp. 43-51.

[24] Gawin D., Pesavento F., Schrefler B.A., Modelling of Hygro-Thermal Behaviour and Damage of Concrete at Temperature Above the Critical Point of Water, *Int. J. Numer. Anal. Meth. Geomech.*, Vol 26, 2002, pp. 537-562.

[25] Khoury G., Majorana C.E., Pesavento F., Schrefler B.A., Thermo-hydro-mechanical modelling of high performance concrete at high temperatures, *Mag. of Concr. Res.*, Vol 54, No 2, 2002, pp. 77-101.

[26] Gawin D., Pesavento F., Schrefler B.A., Simulation of damage-permeability coupling in hygro-thermo-mechanical analysis of concrete at high temperature, *Comm. Numer. Meth. Engrg*, Vol. 18, No 2, 2002, pp 113–119.

[27] Bianco M., Bilardi G., Pesavento F., Pucci G., Schrefler B.A., A frontal solver tuned for fully-coupled non-linear hygro-thermo-mechanical problems, *Int. J. of Numer. Meth. Engrg*, Vol 57, No 13, 2003, pp. 1801-1818.

[28] Gawin D., Pesavento F., Schrefler B.A., Towards prediction of the thermal spalling risk through a multi-phase porous media model of concrete, *Comput. Methods Appl. Mech. Engrg.*, 2006, Vol. 195, pp. 5707–5729

[29] Gawin D., Pesavento F., Schrefler B.A., Modelling damaging processes of concrete at high temperature with thermodynamics of multiphase porous media, *J. of Theor. Appl. Mech.*, Vol. 44, No 3, 2006, pp. 505–532.

[30] Phan L.T., Lawson J.R., Davis F.L., Effects of elevated temperature exposure on heating characteristics, spalling, and residual properties of high performance concrete, *Materials and Structures,* Vol. 34, 2001, pp. 83-91.

[31] Phan L.T., Carino N.J., Effects of test conditions and mixture proportions on behavior of high-strength concrete exposed to high temperature, *ACI Materials Journal*, Vol 99, No 1, 2002, pp. 54-66.

[32] Phan L.T., *Fire performance of high-strength concrete: a report of the state-of-the-art*, Res. Report NISTIR 5934, pp.105, National Institute of Standards and Technology, Gaitherburg, 1996.